Journal of Materials Chemistry A

Accepted Manuscript

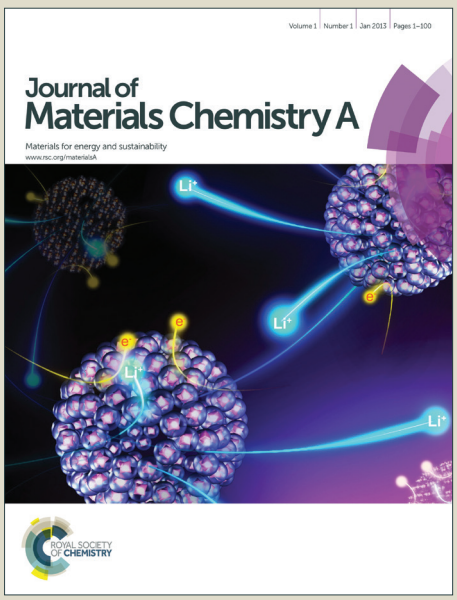

ROYAL SOCIETY OF CHEMISTRY

www.rsc.org/materialsA

Journal Name

RSCPublishing

ARTICLE

Improved dehydrogenation performance of $LiBH_4$ by confining into porous TiO_2 micro-tubes

Cite this: DOI: 10.1039/xoxxoooooox

Huiqiao Liu, Lifang Jiao*, Yanping Zhao, Kangzhe Cao, Yongchang Liu, Yijing Wang, Huatang Yuan

Received ooth January 2012,
Accepted ooth January 2012

DOI: 10.1039/xoxxoooooox

www.rsc.org/

Porous TiO_2 micro-tubes were fabricated by solvothermal method and the effect of TiO_2 micro-tubes on hydrogen desorption properties of $LiBH_4$ was systematically investigated. It was confirmed that $LiBH_4$ nanoparticles were successfully incorporated into these TiO_2 scaffolds via a chemical impregnation method. It was revealed by results of TPD, PCT and DSC that both lowering the desorption temperature and improving kinetics of desorption rate were owing to the synergistic effects of nanoconfinement and destabilization of TiO_2. The $LiBH_4$@$2TiO_2$ mixture (the preparation mass ratio is 1:2) started to release hydrogen at 180 °C, and the apparent activation energy (Ea) had been reduced from 146 kJ/mol (pure $LiBH_4$) to 121.9 kJ/mol. And it is interesting that the onset desorption temperature of $LiBH_4$@$3TiO_2$ composite was below 100 °C, reduced by about 300 °C compared to that of pure $LiBH_4$, which was lower than most of the current studies about $LiBH_4$.

1 Introduction

Hydrogen, due to its clean combustion and potentially renewable nature, has been regarded as a promising energy source. However, hydrogen storage is one of the most challenging barriers to realize the widespread commercialization of hydrogen-fueled vehicles.[1] Recently, complex hydrides, such as alanates (AlH_4^-),[2-4] amides (NH_2^-),[5, 6] and borohydrides (BH_4^-)[7-10] have been investigated intensively because of their high hydrogen content and their associated use for hydrogen storage. Among these complex hydrides, lithium borohydride has a gravimetric capacity of 18.5 wt% and may be a promising candidate for onboard applications. However, it is too thermodynamically stable to decompose at ambient condition and reversibility requires pressures too high for practical applications.[11] According to the literature,[24] the transition temperature of $LiBH_4$ from the orthorhombic to the hexagonal is around 110 °C and the melting transition is about 270 °C. When heated to 600 °C, the following reaction occurs:

$$LiBH_4 \rightarrow LiH + B + 3/2H_2$$

Several methods have been adopted to improve the dehydrogenation properties of $LiBH_4$. Doping additives, such as metal oxides, halides, hydrides and amides, has been focused to lower the dehydrogenation temperature of $LiBH_4$.[12-16] Yu and co-workers added SiO_2 to $LiBH_4$, showing that the addition of SiO_2 to $LiBH_4$ lowered the hydrogen desorption temperatures significantly.[17] It is reported by Kyle Crosby. that the onset dehydrogenation temperature of $LiBH_4$ was reduced to below 300 °C after ball milling with MgH_2,[18] and according to Chen's work,[19] direct hydrogen liberation from the interaction of $LiBH_4$ and NH_3 was to be 17.8 wt% in the temperature range from 135 °C to 250 °C with the assistance of Co catalyst.

There were also some researchers attempting to reduce the size of materials to nanoscales to alter the kinetics and thermodynamics of hydrogen storage materials.[20, 21] However, the practical application of this approach can be limited by growth and agglomeration of particles during cycling. Recent literature reports showed that confining the hydrogen storage material in a scaffold host was beneficial. In this way, grain growth and particle agglomeration can be limited effectively

Institute of New Energy Material Chemistry, Collaborative Innovation Center of Chemical Science and Engineering (Tianjin), Key Laboratory of Advanced Energy Materials Chemistry (MOE), Tianjin Key Lab of Metal and Molecule-based Material Chemistry, Nankai University, Tianjin 300071, P.R. China, Email: jiaolf@nankai.edu.cn. Fax: +86 22 23502604; Tel.: +86 22 23504527

† Electronic Supplementary Information (ESI) available: [Fig. S1-S2]. See DOI: 10.1039/b000000x/

during cycling. What's more, fast kinetics may occur due to shorter diffusion paths. According to Cahen. *et al*.,[22] $LiBH_4$/carbon composites were obtained by impregnation of the carbon matrix with $LiBH_4$ solubilized within ethers, and $LiBH_4$/carbon composites showed excellent desorption kinetics with a hydrogen release of 3.4wt.% in 90 min at 300 °C. Peter Ngene *et al*.[20] also investigated that the confined $LiBH_4$ had enhanced hydrogen desorption properties, which desorption starting at 150 °C.

However, it is a challenge to achieve the requirements of practical applications if the above methods were adopted separately. Here, we present a method that take advantage of the synergic action of nanoconfinement and destabilization to enhance the desorption performance of $LiBH_4$. During nanoconfinement process, the confined carrier itself can also act as the destabilization agent. And it can not only inhibit the growth and agglomeration of particles, but also give full play to destabilize $LiBH_4$. So this method has a great potential to improve the dehydrogenation of hydrides. In this report, we synthesized porous TiO_2 microtubes and successfully confined $LiBH_4$ nanoparticles within these scaffolds, hoping to take advantage of synergistic effect of nanoconfinement and destabilization effects of TiO_2 to improve the dehydrogenate properties of $LiBH_4$. In addition, the dehydrogenation performances and mechanism were investigated.

2. Experimental Method

$LiBH_4$ (95%) was purchased from Acros, $TiOSO_4$, ethanol (99.7%), glycerol (99%), ethyl ether (99%) and tetrahydrofuran (THF, 99.8%) were purchased from Guangfu technology company of Tianjin. All the other reagents were used as received besides THF need to be distilled.

Preparation of TiO_2 micro-tubes

Porous TiO_2 micro-tubes were synthesized *via* a solvothermal method according to the previously procedures.[23] In a typical synthesis, 0.3120 g $TiOSO_4$ was added into a solvent containing 30 ml of ethanol, 15 ml of glycerol and 15 ml of ethyl ether. After stirring for 1 h, the solution was transferred into a 100 ml Teflon-linedstainless steel autoclave and maintained at 110 °C for 48 h for a hydrothermal reaction. The resulted white precipitate was centrifuged, washed thoroughly with distilled water and anhydrous alcohol, and then dried in a vacuum oven at 80 °C overnight, followed by a further thermal treatment at 550 °C in an air atmosphere for 6 h.

Preparation of $LiBH_4$@xTiO_2 composites

To prepare $LiBH_4$@TiO_2 (the preparation mass ratio is 1:1), 0.200 g of $LiBH_4$ was dissolved in anhydrous THF with the ratio of 2 ml THF/0.1 g $LiBH_4$. After full dissolution, the solution was injected into a three nected-flask with TiO_2 put in advance and the TiO_2 was vacuum treatment ahead of time. The whole reaction unit was attached to a Schlenk line. After stirring for 6 h, the mixture was treated by heating to remove the THF residue. All handling of the samples were carried out in the glove box (Mikrouna Co., China) under purified argon atomosphere (H_2O<1ppm; O_2<1ppm). The other $LiBH_4$@xTiO_2 (x=2, 3) composites were prepared in the same way. As a control sample, pure TiO_2 was also disposed by the same method.

Characterization

The phase structure and morphology of the materials were characterized by X-ray diffraction (XRD, Rigaku D/Max-2500, Cu Kα radiation), scanning electron microscopy (SEM, Hitachi X-650) and transmission electron microscopy (TEM Tecnai 20). X-ray diffraction (XRD) patterns were recorded at a scanning rate of 4° min^{-1} in a 2θ range of 10° to 80° under identical conditions. For XRD studies, all the nanocomposite samples were smeared on a glass slide in an argon glove box and then covered with parafilm tape for the avoidance of moisture and oxygen contact during the measurement. N_2 adsorption-desorption isotherms were measured with Quantachrome Instruments (NoVA 2200e) and the N_2 desorption temperature was 50°C. The pore size distributions were obtained from the adsorption branches of the isotherms using the Barrette-Joynere-Halenda (BJH) method and the surface areas were calculated by the Brunauere-Emmette-Teller (BET) method. FT-IR spectra were collected at room temperature via a FT-IR-650 spectrometer (Tianjin Gangdong) at a resolution of 4 cm^{-1}. X-ray photoelectron spectrometer (XPS, PHI 5000 Versaprobe, ULVAC PHI) was also used to characterize the dehydrogenated materials. The actual loadings of $LiBH_4$ in the resulted $LiBH_4$@xTiO_2 samples were deduced from the measurements of Li contents through inductively coupled plasma atomic emission spectroscopy (ICP-AES) using a USA Themo Jarrel-Ash Corp instrument. The dehydrogenation behaviors of the samples were measured under flowing argon (about 35.0 ml min^{-1}) in a home-made temperature programmed desorption (TPD) system at a ramping rate of 2 °C min^{-1} in the temperature range from 30 °C to 600 °C. Kinetics performances were examined by Sieverts-type isothermal measurement at different temperatures using a volumetric method. DSC analysis was conducted on TA instruments to obtain the activation energy of the samples.

3. Results and discussion

Structural and morphology characterization

The morphologies of the as-prepared TiO_2 and $LiBH_4$@TiO_2 composites were demonstrated in Fig. 1. Fig. 1a gives an overall view of TiO_2 microtubes, of which the walls are made of interconnected particles. And large numbers of mesopores also present (see Fig. 1b). It is this unique porous structure that provides the possibility of confining $LiBH_4$ nanoparticles. From Fig. 1c, the outer and inner diameters of the tubular materials are measured to be around 1 μm and 0.8 μm, respectively. While, as it can be seen from the TEM of $LiBH_4$@TiO_2 composite displayed in Fig. 1e, the micro-tube structure still exists and the pipe thickness increases to 0.5 μm, which can be

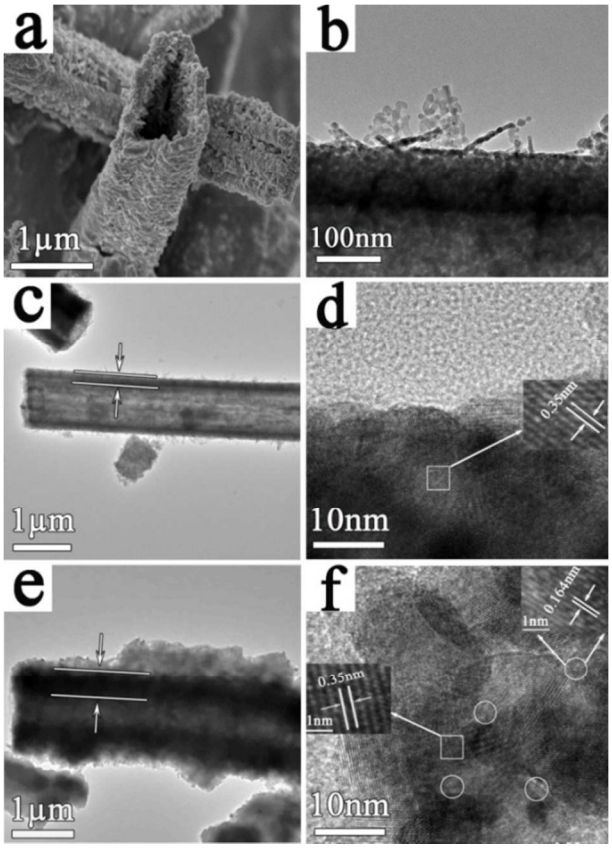

Fig. 1 (a) SEM of the as-prepared TiO_2, (b)、(c) TEM and (d) HR-TEM of the as-prepared TiO_2, (e) TEM and (f) HR-TEM of $LiBH_4$@TiO_2 composites (the mass ratio of $LiBH_4$ and TiO_2 is 1:1).

attributed to the appearance of $LiBH_4$ nanoparticles inside and outside the porous tube walls. The fact that TiO_2 frameworks are not destroyed during the nanoconfinment process indicating that it is feasible to choose this scaffold as confined carrier. From the HR-TEM image (Fig. 1d) taken from the selected area, the spacing of the lattice fringes is calculated to be 0.35 nm, corresponding well to the d-spacing for the (101) plane of TiO_2 anatase phase. While, except the above lattice fringes, a weak lattice fringe of 0.164 nm is also measured among $LiBH_4$@TiO_2 composite as Fig. 1f presents. Interestingly, these lattice fringes are completely consistent with the (300) planes of tetragonal $LiBH_4$. What's more, those lattice fringes distribute among TiO_2 nanoparticles. It is well verified that the $LiBH_4$ granules are confined into porous TiO_2 tube walls.

To further demonstrate the confinement of TiO_2 carriers, the pore size distributions, pore volumes and BET surface area of

Table 1 Values of pore diameter, pore volume and BET surface area of TiO_2 and $LiBH_4$@xTiO_2 samples

Samples	Pore Diameter (nm)	Pore Volume (cm^3/g)	BET surface area (m^2/g)
$LiBH_4$@TiO_2	3.80	0.030	5.4
$LiBH_4$@2TiO_2	3.82	0.062	11.0
$LiBH_4$@3TiO_2	7.66	0.218	76.8
TiO_2	7.79	0.258	95.1

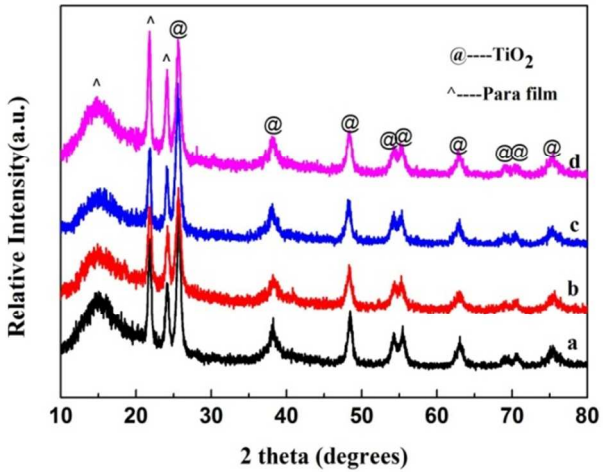

Fig. 2 X-ray diffraction patterns of (a) as-prepared TiO_2, (b) $LiBH_4$@TiO_2, (c) $LiBH_4$@2TiO_2, and (d) $LiBH_4$@3TiO_2 composites.

$LiBH_4$@xTiO_2 composites and pure TiO_2 are conducted and display in Fig. S1 of supporting information, and the relative values are listed in table 1. From the figures we can see that when incorporated by $LiBH_4$ nanoparticles, the pore diameter, pore volume and BET surface area of TiO_2 all appear declining trends. With increasing amount of $LiBH_4$ in the mixture, the pore sizes of composites gradually decreasing. So it can be concluded that a part of $LiBH_4$ particles have been incorporated into TiO_2 micro-tubes.

Fig. 2 represents the powder X-ray diffraction patterns of the as-prepared TiO_2 and $LiBH_4$@xTiO_2. The phase of the as-prepared TiO_2 can be indexed to anatase (JCPDS 1-562), indicating that a pure phase of TiO_2 has been obtained from the original material of $TiOSO_4$ by a solvothermal method. The diffraction peaks of all $LiBH_4$@xTiO_2 composites bear similar to those of pure TiO_2. According to Peter Ngene,[20] no specific reflections of $LiBH_4$ indicates that the clusters are amorphous and present in TiO_2 micro-tubes.

Hydrogen desorption properties

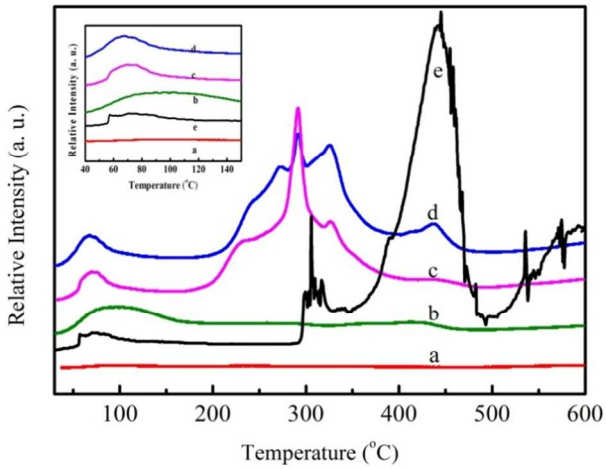

Fig. 3 TPD dehydrogenation curves of (a) pure TiO_2, (b) $LiBH_4$@3TiO_2, (c) $LiBH_4$@2TiO_2, (d) $LiBH_4$@TiO_2 and (e) bulk $LiBH_4$.

Fig. 3 shows TPD curves of the $LiBH_4$@xTiO_2 composites, pure TiO_2 and bulk $LiBH_4$. From TPD curves of bulk $LiBH_4$ (see Fig. 3a), we can get that it shows multiple desorption peaks. The onset dehydrogenation temperature of bulk $LiBH_4$ is around 275 °C, close to its melting point, and the majority of the hydrogen is only released above 400 °C. While, compared with the multiple desorption peaks of pure $LiBH_4$, the composites of $LiBH_4$@xTiO_2 tend to be a unimodal pattern during dehydrogenation, especially for $LiBH_4$@2TiO_2. And the dehydrogenation temperatures of $LiBH_4$ decrease obviously. For $LiBH_4$@TiO_2 and $LiBH_4$@2TiO_2, the starting hydrogen release temperatures are around 193 °C and 180 °C, respectively, and the main dehydrogenation temperatures are around 290 °C. While only a broaden peak at 50~150 °C appears in the TPD curves of $LiBH_4$@3TiO_2. When the amount of $LiBH_4$ is above 23 wt%, the pores of TiO_2 are fully filled, and naturally some bulk $LiBH_4$ is outside the pores. Certainly, an inferior peak around 440 °C is observed from the TPD dehydrogenation curve of $LiBH_4$@TiO_2, which is similar to that of bulk $LiBH_4$. In addition, there is a weak peak occurring at around 70 °C in Fig. 4. As reported by Guo *et al*,[10] this peak may attribute to the volatilization of little THF residue in the sample. However, in our work, without dissolving in THF, the dehydrogenation curves of bulk $LiBH_4$ also appears the weak peak at about 70 °C. And we can't observe any peaks from TPD curve of TiO_2 in Fig. 3a. Therefore, the weak peak of $LiBH_4$@xTiO_2 composites related neither to THF nor to TiO_2. It is corresponded to the phase transformation of $LiBH_4$.

The quantification of the total amount of hydrogen release evaluated is given in Fig. 4. As is shown in the insert chart of Fig. 4, due to the presence of TiO_2 in samples, the total amount of hydrogen desorbed from $LiBH_4$@xTiO_2 composites is far lower than pure $LiBH_4$. While, through the curves that hydrogen released calculate from pure $LiBH_4$, we can see that the dehydrogenation rates of samples ($LiBH_4$@xTiO_2) gradually increase with the amount of TiO_2 from 0 to 3 below150 °C. After heating to 150 °C, the dehydrogenation rate of $LiBH_4$@3TiO_2 slows down and the final hydrogen production is less than others. However, it is inspiring that most of materials start to release hydrogen around 200 °C. The hydrogen release characteristics of all the above samples are summarized in Table 2.

Table 2 Hydrogen release characteristics of $LiBH_4$@xTiO_2 samples

Sample	Temperature at the major H2 release(°C)		Actual weight loadings of LiBH4/wt%	Calculated H2 released from LiBH4 at 600 °C /wt%
	onset	peak		
bulk LiBH4	294	445	100	13.7
LiBH4@TiO2	194	292	25.856	14.658
LiBH4@2TiO2	183	291	22.969	14.715
LiBH4@3TiO2	——	100	13.578	8.5

In order to investigate the kinetic properties of $LiBH_4$ in $LiBH_4$@xTiO_2 composites, the isothermal hydrogen desorption measurements are conducted. As it displays in Fig. 5, the hydrogen desorption rates are significantly higher for $LiBH_4$@xTiO_2 composites compared with pure $LiBH_4$, especially during the first 60 min of measurements. What's more, with the increasing amount of TiO_2 in the composites, the dehydrogenation kinetic performances are gradually improved. It is noteworthy that $LiBH_4$ in $LiBH_4$@3TiO_2 composite reached the maximum dehydrogenation platform in 15 min at 310 °C, and $LiBH_4$ in $LiBH_4$@2TiO_2 composite finishes hydrogen desorption during the initial one hour. While, there are no obviously platforms for $LiBH_4$@TiO_2composite and bulk $LiBH_4$ during the whole measurement time. Meanwhile, the dehydrogenation capacities of pure $LiBH_4$, $LiBH_4$@TiO_2, $LiBH_4$@2TiO_2 and $LiBH_4$@3TiO_2 in 60 min at 310 °C are 0.43 wt%, 1.00 wt%, 2.47 wt% and 0.71 wt%, respectively. The inferior desorption weights are related to the low content of $LiBH_4$ in the composites. But it is encouraging to see that

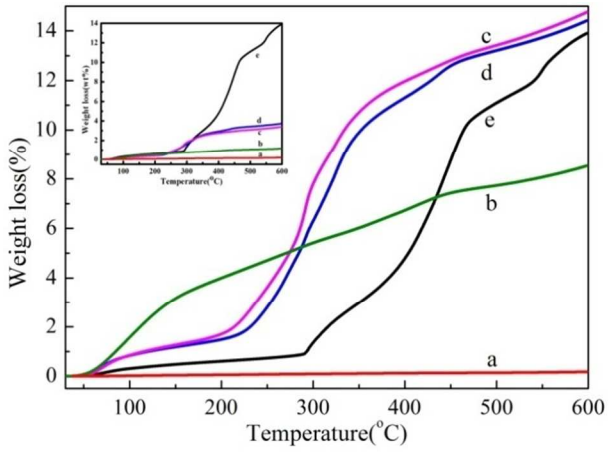

Fig. 4 Hydrogen weight loss of (a) TiO_2, (b) $LiBH_4$@3iO_2, (c) $LiBH_4$@2TiO_2, (d) $LiBH_4$@TiO_2 and (e) pure $LiBH_4$ calculated H_2 released from $LiBH_4$ and from $LiBH_4$@xTiO_2 composites (inside chart) at 600 °C.

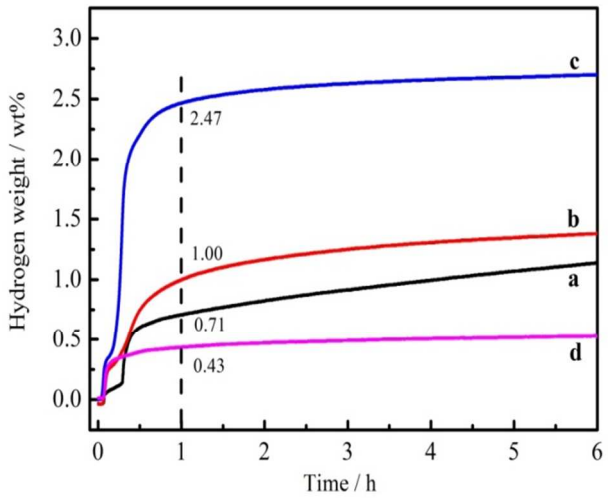

Fig. 5 Hydrogen release from (a) pure $LiBH_4$, (b)$LiBH_4$@TiO_2, (c) $LiBH_4$@2TiO_2, (d) $LiBH_4$@3TiO_2 at 310 °C.

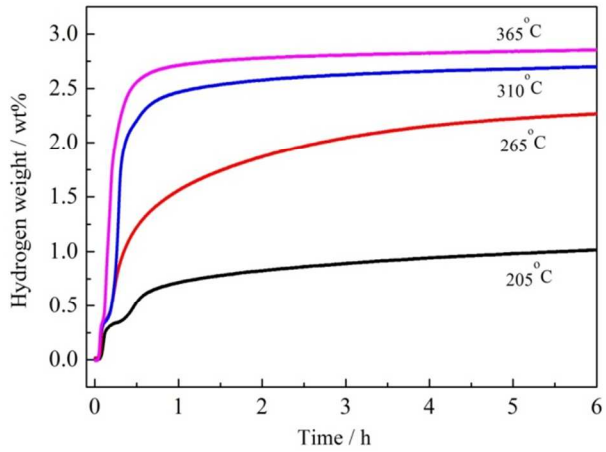

Fig. 6 Isothermal hydrogen desorption profiles of $LiBH_4$@$2TiO_2$ composite at different temperatures.

$LiBH_4$ in $LiBH_4$@$2TiO_2$ composite shows a superior performance compared to other two composites. Considering both lower desorption temperature and higher hydrogen capacity, we choose $LiBH_4$@$2TiO_2$ for further investigations.

To investigate the effect of as-prepared TiO_2 on desorption rate of $LiBH_4$, experiments of $LiBH_4$@$2TiO_2$ sample dehydrogenated at 205 °C, 265 °C, 310 °C and 365 °C are operated respectively. From Fig. 6, we can project that as the temperature increase from 205 °C to 365 °C, the decomposition kinetics augment gradually, leading to the improvement in reactivity. 2.8 wt% of hydrogen is released from $LiBH_4$@$2TiO_2$ within 1 h at 365 °C, which corresponds to 10.8 wt% when calculated by pure $LiBH_4$.

To further shed light on the kinetics of $LiBH_4$@$2TiO_2$ sample, the apparent activation energy (Ea) related to the dehydrogenation is calculated according to the following equation (Kissinger method):

$$\frac{d\ln(\beta/T_m^2)}{d(1/T_m)} = \frac{E_a}{R}$$

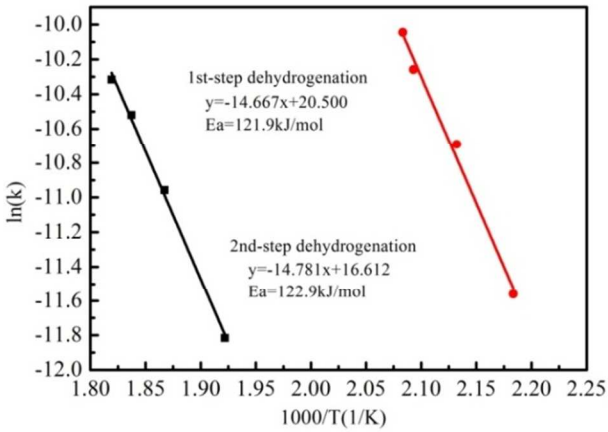

Fig. 7 Kissinger plots of the dehydrogenation of $LiBH_4$@$2TiO_2$ composite.

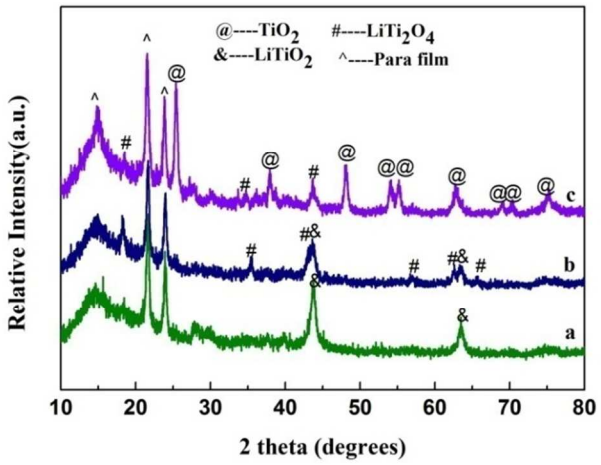

Fig. 8 XRD pattern of (a) $LiBH_4$@TiO_2, (b)$LiBH_4$@$2TiO_2$, (c) $LiBH_4$@$3TiO_2$ composites after dehydrogenation at 600 °C.

Where, β is the heating rate, T_m is the absolute temperature for the maximum desorption rate and R is the gas constant. In addition, T_m is obtained using DSC measurements with the heating rates of 2, 5, 8, 10 °C min^{-1}, which display in Fig. S2 (supporting information). Fig. 7 shows the Kissinger plots of the dehydrogenation of $LiBH_4$@$2TiO_2$ composite. The activation energy (Ea) for the mixture is calculated to be 121.9 kJ/mol of first step and 122.9 kJ/mol of second step. These values are much lower than that of pure $LiBH_4$ (146 kJ/mol) in the literature,[25] which indicates that the synergistic effect between nanoconfinement and destabilization of TiO_2 has enhanced desorption kinetics of $LiBH_4$ greatly.

Deduction of the dehydrogenation mechanism

Fig. 8 displays the XRD patterns of $LiBH_4$@xTiO_2 composites after dehydrogenation at 600 °C. The materials with different mass ratios between TiO_2 and $LiBH_4$ have different diffraction peaks after dehydrogenation. For $LiBH_4$@TiO_2, the main peaks are attached to $LiTiO_2$. While, apart from the $LiTiO_2$ phase, there appears $LiTi_2O_4$ phase in the dehydrogenated products of $LiBH_4$@$2TiO_2$ composite. From above results, it can be inferred that during the hydrogen desorption process, following reactions may occur:

$$TiO_2 + LiBH_4 \rightarrow LiTiO_2 + B + 2H_2\uparrow \quad (1)$$
$$2TiO_2 + LiBH_4 \rightarrow LiTi_2O_4 + B + 2H_2\uparrow \quad (2)$$

With the increasing amount of TiO_2, the final products are gradually altered from $LiTiO_2$ to $LiTi_2O_4$. When adding more amount of TiO_2 to the composite, taking $LiBH_4$@$3TiO_2$ for example, the ultimate products are the mixture of TiO_2 and $LiTi_2O_4$. Therefore, the main dehydrogenation product of $LiBH_4$@xTiO_2 composites is $LiTi_xO_y$.

In order to have a better understand of the effect of TiO_2 on the dehydrogenation process of $LiBH_4$, XRD patterns and FT-IR spectra of $LiBH_4$@$2TiO_2$ composite and its dehydrogenated

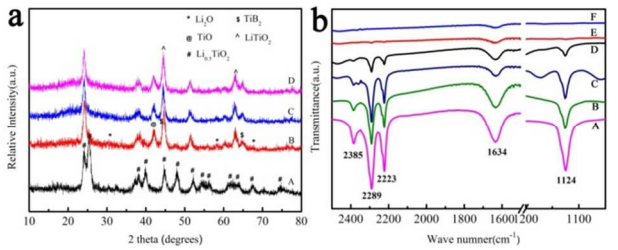

Fig. 9 (a) XRD patterns of dehydrogenated of $LiBH_4$@$2TiO_2$ sample at (A) 205 °C, (B) 265 °C, (C) 310 °C and (D) 365 °C; (b) FT-IR spectra of (A) pure $LiBH_4$, (B) $LiBH_4$@$2TiO_2$ composite and its dehydrogenated products at (C) 205 °C, (D) 265 °C, (E) 310 °C, (F) 365 °C.

products at different temperatures are conducted and present in Fig. 9. In the FT-IR spectrum, typical B-H vibrations in $LiBH_4$ are observed at 2385, 2289, 2223, 1634 and 1124 cm^{-1}, [19, 26] confirming the emergence of $LiBH_4$ in the $LiBH_4$@$2TiO_2$ composite. Moreover, the absorbance intensities of B-H detected gradually become weak with the heating temperature rising and completely vanish when heating above 310 °C. Meanwhile, the XRD patterns of $LiBH_4$@$2TiO_2$ show different peaks after desorption at various temperatures. When heating at a lower temperature, taking 205 °C for example, $Li_{0.5}TiO_2$ is detected as the mean product. As temperature raises, the ultimate products are $Li_{0.5}TiO_2$ and $LiTiO_2$, in addition, a trace amount Li_2O, TiB_2 and TiO can also be detected. The above results show that a redox reaction has taken place during the dehydrogenation process of $LiBH_4$@xTiO_2 composites.[2, 27] Chemical states of titanium are characterized by XPS for further investigation. As is shown in Fig. 10, the $Ti2p_{3/2}$ peak becomes asymmetric and shifts to lower banding energies with the increasing heating temperature. The Ti $2p_{3/2}$ peaks are range from 459.4 eV to 456.2 eV, which represent titanium species with oxidation states between +3 and +4, illustrating the local chemical environments of Ti have been significantly influenced by the emerged Li ions and the forming of Li_xTiO_y phase due to the redox reaction.[28-31]

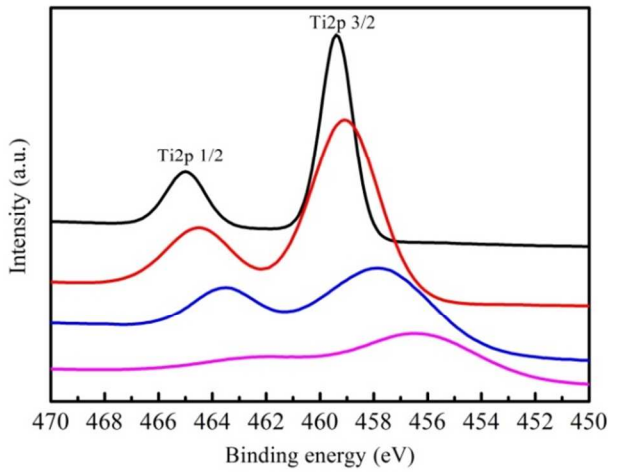

Fig. 10 XPS of dehydrogenated products of $LiBH_4$@$2TiO_2$ sample at (a) 205 °C, (b) 265 °C, (c) 310 °C and (d) 365 °C.

In summary, the dehydrogenation mechanism may be ascribed as following. First, the porous TiO_2 tube can act as carrier to confine $LiBH_4$, thus TiO_2 can not only contact directly to $LiBH_4$ granules, also inhibit the growth and agglomeration of particles. Then, when heating, $LiBH_4$ granules would react with the TiO_2 support that around them. The porous structure of TiO_2 can introduce a large amount of reaction nucleation sites and hydrogen diffusion channels for the dehydrogenation process. Simultaneously, the formation of Li-Ti oxide suggests that Ti^{4+} has been reduced to lower valance state, and hydrogen released during this process. What's more, the TiO_2 support can prevent the hydrogenation products from agglomeration during the whole dehydrogenation process, which may contribute to the improved desorption kinetics.

3 Conclusions

In this study, we successfully synthesized porous micro-tube structure TiO_2. Experiment results show that the frameworks are not destroyed when $LiBH_4$ incorporated into TiO_2 scaffold host via a chemical impregnation method, which indicate that choosing this scaffold as confined carrier is feasible. Simultaneously, the dehydrogenation properties of $LiBH_4$ are significantly enhanced after being confined into TiO_2 scaffold. The onset dehydrogenation temperature for $LiBH_4$@$2TiO_2$ is reduced to 180 °C, and the maximal desorption peak occurs at about 290 °C. Meanwhile, the dehydrogen temperature of $LiBH_4$@$3TiO_2$ is around 100 °C, which is much lower than that of the bulk $LiBH_4$. What's more, the apparent activation (Ea) has reduced to 121.9 KJ/mol. And the desorption mechanism investigation of $LiBH_4$@$2TiO_2$ indicates that the products are ranged from $Li_{0.5}TiO_2$ to $LiTiO_2$ as heating temperature raises.

Acknowledgements

The authors gratefully acknowledge the financial support for this research from 973 program (2010CB631303), NSFC (51171083), MOE Innovation Team (IRT-13R30 and IRT13022) and 111 Project (B12015).

Notes and References

1 L. Schlapbach and A. Züttel, *Nature*, 2001, **414**, 353.
2 Z. L. Li, P Li, Q Wan, F. Q. Zhai, Z. W. Liu, K. F. Zhao, L. Wang, S. Y. Lu, L. Zou, X. H. Qu and A. A. Volinsky, *J Phys Chem C*, 2013, **117**, 18343.
3 L. Li, F. Y. Qiu, Y. P. Wang, Y. J. Wang, G. Liu, C. Yan, C. H. An, Y. N. Xu, D. W. Song, L. F. Jiao and H. T. Yuan, *J. Mater. Chem.*, 2012, **22**, 3127.
4 M. Ismail, Y. Zhao, X. B. Yu, I. P. Nevirkovets, and S. X. Dou, *Int. J. Hydrogen Energy*, 2011, **3**, 8327.
5 Y. F. Liu, C. Li, B. Li, M. Gao and H. G. Pan, *J Phys Chem C*, 2013, **117**, 866.

6 J. H. Wang, G. T. Wu, Y. S. Chua, J. P. Guo, Z. T. Xiong, Y. Zhang, M. X. Gao, H. G. Pan and P. Chen, *ChemSusChem*, 2011, **4**, 1622.
7 J. Xu, R. R. Meng, J. Y. Cao, X. F. Gu, Z. Q. Qi, W. C. Wang and Z. D. Chen, *Int. J. Hydrogen Energy*, 2013, **38**, 2796.
8 P. Ngene, M. V. Zwienen and P. E. Jongh, *Chem. Commun.*, 2010, **46**, 8201.
9 S. Cahen, J. B. Eymery, R. Janot and J. M. Tarascon, *J. Power Sources*, 2009, **189**, 902.
10 L. J. Guo, L. F. Jiao, L. Li, Q. H. Wang, G. Liu, H. M. Du, Q. Wu, J. Du, J. Q. Yang, C. Yan, Y. J. Wang and H. T. Yuan, *Int J Hydrogen Energy*, 2013, **38**, 162.
11 M. Au, A. R. Jurgensen, W. A. Spencer, D. L. Anton, F. E. Pinkerton, S. J. Hwang, C. Kim and R. C. Bowman, *J Phys Chem C*, 2008, **112**, 18661.
12 X. L. Si, F. Li, L. X. Sun, F. Xu, S. S. Liu, J. Zhang, M. Zhu, L. Z. Ouyang, D. L. Sun and Y. L. Liu, *J Phys Chem C*, 2011, **115**, 9780.
13 K. Jiang, X. Z. Xiao, L. X. Chen, L. Y. Han, S. Q. Li, H. W. Ge and Q. D. Wang, *J Alloys Compd*, 2012, **539**, 103.
14 H. Maekawa, M. Matsuo, H. Takamura, M. Ando, Y. Noda and T. Karahashi, *J. Am. Chem. Soc.*, 2009, **131**, 894.
15 D. M. Liu, Q. Q. Liu,T. Z. Si, Q. A. Zhang, F. Fang, D. L. Sun, L. Z. Ouyang and M. Zhu, *Chem. Commun.*, 2011, **47**, 5741.
16 M. Q. Fan, L. X. Sun, Y. Zhang, F. Xu, J. Zhang and H. L. Chu, *Int. J. Hydrogen Energy*, 2008, **33**, 74.
17 X. B. Yu, D. M. Grant and G. S. Walker, *J. Phys. Chem. C*, 2009, **113**, 17945.
18 K. Crosby and L. L. Shaw, *Int. J. Hydrogen Energy*, 2010, **35**, 7519.
19 X. L. Zheng, G. T. Wu, W. Li, Z. T. Xiong, T. He, J. P. Guo, H. Chen and P. Chen, *Energy Environ Sci.*, 2011, **4**, 3593.
20 P. Ngene, P. Adelhelm, A. M. Beale, K. P. Jong and P. E. Jongh, *J Phys Chem C*, 2010, **114**, 6163.
21 Z. Zhao-Karger, R. Witter, E. G. Bardaji, D. Wang, D. Cossement and M. Fichtner, *J. Mater. Chem. A*, 2013, **1**, 3379.
22 S. Cahen, J. B. Eymery, R. Janot and J. M. Tarascon, *J. Power Sources*, 2009, **189**, 902.
23 Z. F. Bian, J. Zhu, J. G. Wang, S. X. Xiao, C. Nuckolls, and H. X. Li, *J Am Chem Soc*, 2012, **134**, 2325.
24 H. Maekawa, M. Matsuo, H. Takamura, M. Ando, Y. Noda, T. Karahashi, and Shin-ichi Orimo, *J Am Chem Soc*, 2009, **131**, 894.
25 A. F. Gross, J. J. Vajo, S. L. Van Atta and G. L. Olson, *J. Phys. Chem. C*, 2008, **112**, 5651.
26 Y. F. Zhou, Y. F. Liu, Y. Zhang, M. X. Gao and H. G. Pan, *Dalton Trans*, 2012, **41**, 10980.
27 X. B. Yu, D. M. Grant and G. S. Walker, *J. Phys. Chem. C*, 2008, **112**, 11059.
28 M. Samiee and J. Luo, *J Power Sources*, 2014, **245**, 594.
29 N. D. Feng, Q.G Wang, A. M. Zheng, Z. F. Zhang, J. Fan, S. B. Liu, J. P. Amoureux and F. Deng, *J. Am. Chem. Soc.*, 2013, **135**, 1607.
30 J. Yao, C. Shen, P. Zhang , C. A. Ma, D. H. Gregory and L. Wang, *Electrochem. Commun.*, 2013, **31**, 92.
31 J. Gu, M. X. Gao, H. G. Pan, Y. F. Liu, B. Li, Y. J. Yang, C. Liang, H. L. Fu and Z. X. Guo, *Energy Environ. Sci.*, 2013, **6**, 847.